A closer look at WNT/CTNNB1 signaling

de Man, S.M.A.

Publication date
2023

CHAPTER 7

Addendum

Saskia M.A. de Man[1,2], Jasmijn M. Span[1,2], Sanne C. Lith[1,2], Beau Neep[1,2], Rianne M. Schoon[1,2], Marten Postma[2,3], Mark A. Hink[2,3], Renée van Amerongen[1]

[1] Developmental, Stem Cell and Cancer Biology, Swammerdam Institute for Life Sciences, University of Amsterdam, Amsterdam, The Netherlands

[2] Molecular Cytology, Swammerdam Institute for Life Sciences, University of Amsterdam, Amsterdam, the Netherlands

[3] van Leeuwenhoek Centre for Advanced Microscopy, Swammerdam Institute for Life Sciences, University of Amsterdam, Amsterdam, the Netherlands

In addition to the work from the previous chapters, I supervised several talented students during their bachelor's or master's internship. Part of their work was focused on generating multicolor tools to study interaction between different components of the WNT/CTNNB1 pathway. Here, I want to highlight the progress made, the limitations we ran into, and the possibilities these novel tools provide for future research.

INTRODUCTION

In this thesis we have highlighted some of the questions that still surround the molecular mechanisms of the CTNNB1 destruction complex. Namely, what is its precise composition or stoichiometry, and how is it inhibited when WNT proteins bind their receptoros? Are its members translocated, saturated, dissociated, internalized or do they change their conformation? To further study these questions, we set out to develop our strategy of endogenous tagging and advanced imaging further. We generated multiple constructs and cell lines in which we tagged additional components of the WNT/CTNNB1 pathway, as well as a rapamycin-based system that allows us to study the interactions between these components. Due to time constraints, we did not fully exploit these tools yet. However, I hope that with the firm basis laid here, the next generations of (PhD) students will continue to develop and use these tools to tackle the many open questions surrounding destruction complex composition, stoichiometry and dynamics.

GENERATION OF CRISPR CELL LINES EXPRESSING FLUORESCENT FUSIONS OF DESTRUCTION COMPLEX MEMBERS

In addition to CTNNB1, we attempted to tag several other WNT/CTNNB1 pathway members. The ultimate goal was to generate multicolor lines to test not only the dynamics of these components themselves, but also to study interactions within the destruction complex.

mScI for labelling endogenous proteins

To generate multicolor cell lines, additional fluorescent tags were needed. To this end, we first tagged CTNNB1 with a different fluorescent protein and compared this line to the SGFP2-CTNNB1 cell line generated in Chapter 3. We selected mScarlet-I (mScI) as it is truly monomeric, bright, and has enhanced maturation characteristics (Bindels et al. 2017). The CRISPR/Cas9 pipeline, as established in Chapter 3 was followed and using FACS, mScI-CTNNB1 single cell clones were obtained (Figure 1A). In this FACS experiment, cells expressing mScI-CTNNB1 were more easily identified than those containing SGFP2-CTNNB1 (see Figure 1 Chapter 3). This is most likely due to the lower autofluorescence on the red side of the spectrum. We further characterized one mScI-CTNNB1 single cell clone, which showed an intact transcriptional response to WNT (Figure 1B) as well as similar localization of CTNNB1 and increased intracellular levels in the cytoplasm and nucleus upon WNT3A stimulation (Figure 1C, Movie 1). This validated that the mScI fluorescent tag did not interfere with CTNNB1 protein function and was suitable for live cell microscopy.

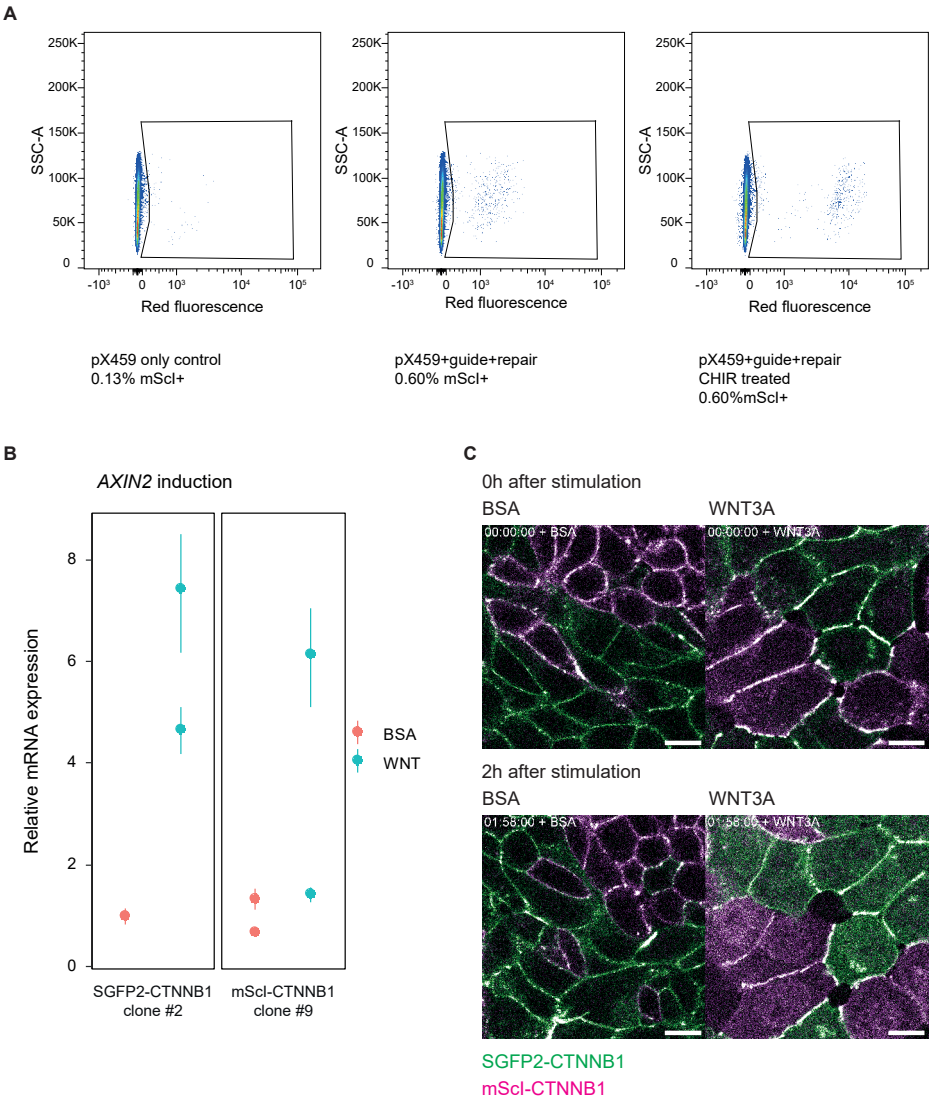

FIGURE 1: mScI-CTNNB1 CRISPR cell line. A) FACS plots showing mScI positive events after CRISPR transfections of pX459 negative control (left) and mScI-CTNNB1 CRISPR constructs (middle & right). The right panel was additionally treated with 8 µM CHIR for 24 hours. Note that CHIR treatment of increased the mScI fluorescence intensity, but not the number of mScI+ events – consistent with data of SGFP2-CTNNB1 in Chapter 3. Several clones positive for mScI-CTNNB1 were identified by PCR and sequenced verified by Sanger Sequencing. Clone #9 was selected for further experiments in B and C. B) Graph depicting the induction of *AXIN2* as measured by qRT-PCR relative to *HPRT* expression (as in Chapter 3) and normalized to untreated SGFP2-CTNNB1 control. Clone SGFP2-CTNNB1 clone #2 and mScI-CTNNB1 clone #9 were treated for 24 hours with 100 ng/ml WNT3A. Vertical lines represent the standard deviation of a technical triplicate, individual data points represent independent biological replicates. C) Representative confocal images from SGFP2-CTNNB1 clone #2 and mScI-CTNNB1 clone #9 that were mixed prior to seeding in a 1:1 ratio. Two hours after treatment with WNT3A cytoplasmic and nuclear accumulation of CTNNB1 can be observed for both colors. Untreated cells from mScI-CTNNB1 and SGFP2-CTNNB1 clones both show localization to cell-cell contacts. Scale bar represents 10 µm.

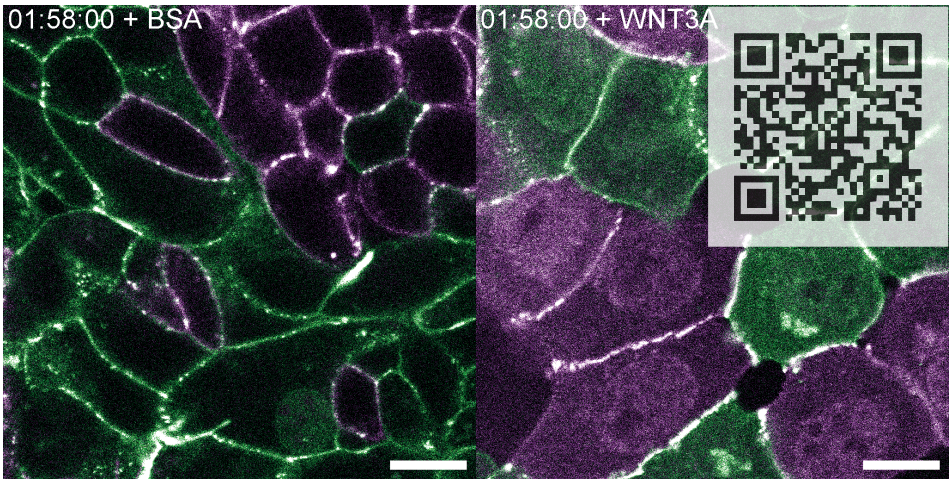

MOVIE 1: SGFP2-CTNNB1 and mScI-CTNNB1 response to WNT3A. mScI-CTNNB1 clone #9 (in magenta) and SGFP2-CTNNB1 clone #2 (in green) were mixed 1:1 at the time of seeding. At the start of imaging, cells were treated with 100 ng/ml WNT3A (right) or BSA control (left), time is indicated in the top left corners, the scale bar represents 10 µm. Use the QR-code to view the movie or visit https://youtu.be/xqAMdlyM4gM.

Tagging multiple proteins

AXIN1

After validating mScI as a suitable fluorescent tag for our purposes, we aimed to generate fusions of additional pathway components using the same CRISPR/Cas strategy. We first focused on AXIN1, as this has typically been described as the rate-limiting component of the destruction complex based on early measurements from Xenopus egg extract (Lee et al. 2003). Although in mammalian systems APC might have lower concentrations (Kitazawa et al. 2017), AXIN1 is still thought of as the main scaffold protein since it directly binds all traditional components (CTNNB1, APC, GSK3 and CSNK1A) (reviewed in van Kappel and Maurice 2017). Outside of AXIN1, many of these other destruction components have additional functions in the cell, which makes them less suitable as an exclusive destruction complex marker. For example, APC is also involved in cytoskeleton regulation (reviewed in Hankey et al. 2018), CSNK1A and GSK3 have many substrates in addition to CTNNB1 (reviewed in Jiang et al. 2018; Robertson et al. 2018) and CTNNB1 itself is also a part of the adherens junction (reviewed in Valenta et al. 2012).

Despite many efforts, we were unable to tag AXIN1 using the pipeline we had set up for CTNNB1. Perhaps the low expression level of AXIN1 is associated with inaccessible chromatin at the *AXIN1* locus and therefore genome editing did not occur, or - in case of successful tagging - fluorescently tagged AXIN1 may be so lowly expressed that the signal could not be detected by FACS (Figure 2). In fact, in a verified AXIN1-mCherry HEK293 cell line, which we kindly received from the lab of Madelon Maurice, we were also unable to

detect fluorescent signal using confocal microscopy, indicating that the latter might well be the case (data not shown).

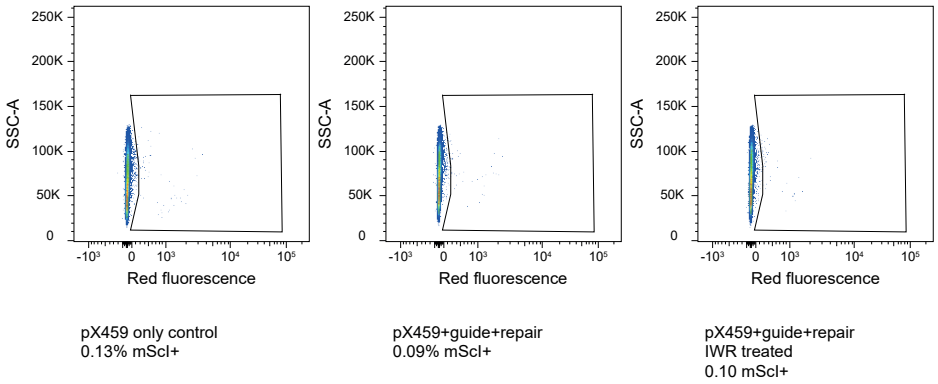

FIGURE 2: Unsuccessful tagging attempt for AXIN1-mScI. FACS plots showing mScI fluorescence after CRISPR transfections of pX459 negative control (left) or AXIN1-mScI CRISPR constructs (middle & right). Transfection with full CRISPR constructs did not show the expected increase of mScI+ events compared to the control. The right panel was additionally treated with 5 μM IWR-001 (a potent tankyrase inhibitor that increases AXIN1 levels) for 24 hours, but this did not increase the fluorescence intensity or population size. Sorting of the mScI+ population of this experiment did not lead to identification of any positive AXIN1-mScI cells by PCR.

APC

As AXIN1 tagging was unsuccessful, we next developed CRISPR constructs for APC, the other scaffold of the destruction complex. A proof of principle experiment in HEK293 cells showed that we could successfully tag APC with mScI in these cells (Figure 3A-B). Three different gates were applied to select for the different ranges of intensities observed after transfection of the CRISPR constructs, and the gate with the lowest mScI intensity, showed the highest integration of mScI at the endogenous APC locus (Figure 3A-B). This population containing APC-mScI cells showed *AXIN2* induction upon treatment with WNT3A or CHIR99021, suggesting that the transcriptional WNT/CTNNB1 response had remained intact (Figure 3C). Confocal imaging revealed that APC-mScI was localized in the cytoplasm, as well as at the membrane (Figure 3D). This is consistent with its role in the cytoskeleton (reviewed in Hankey et al. 2018). It has also been described that membrane recruitment of APC plays an important role in the WNT pathway, as it can localize the destruction complex to the WNT receptor complex, where it is inactivated (Parker and Neufeld 2020). Upon Sanger sequencing of the targeted locus in DNA from subsequently isolated single cell clones, we observed indels at the C-terminus of APC. This is likely due to the fact that the gRNA binding site used for Cas9 targeting and cutting was not mutated in the repair construct, resulting in recutting of the repaired locus leading to in frame indels. Therefore, mutation of this site in the APC-mScI repair plasmid would be required. This altered repair plasmid can then be used to generate new (clonal) cell lines without any additional CRISPR scars. These lines

could subsequently be used to study the dynamics of APC in the destruction complex and its role in destruction complex relocalization.

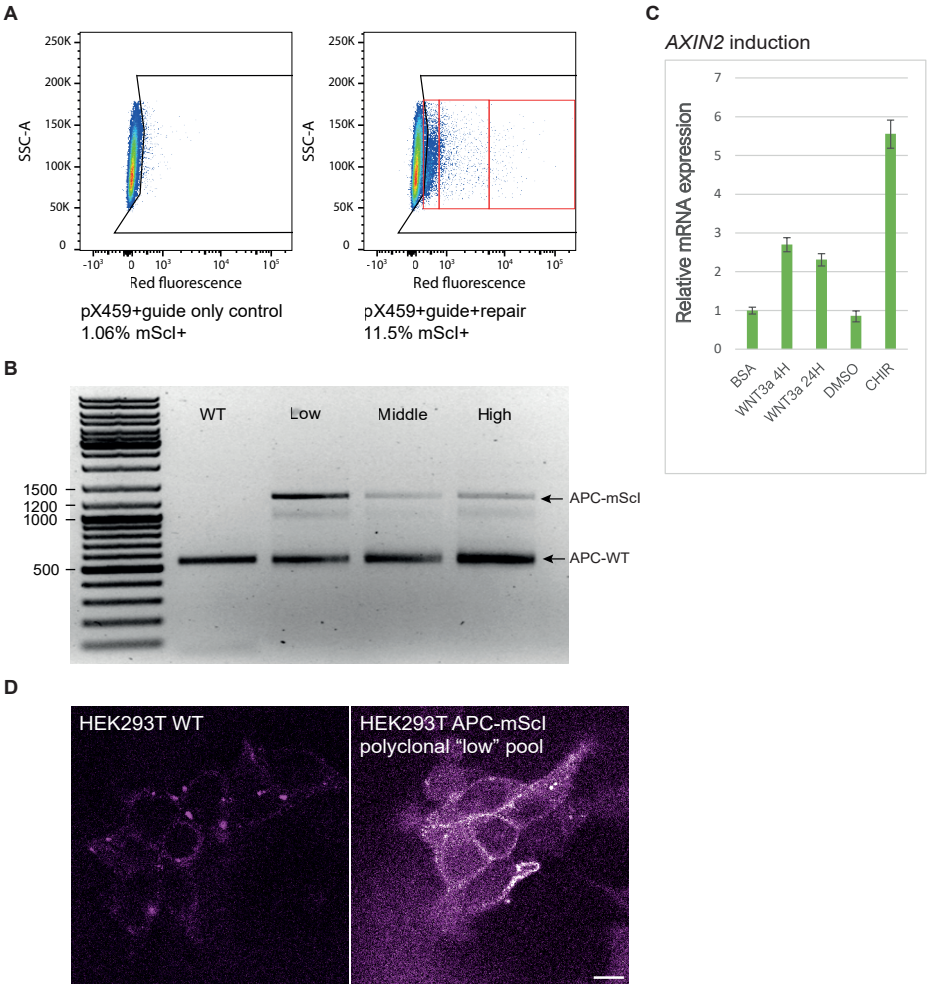

FIGURE 3: APC-mScI CRISPR knock-in in HEK293. A) FACS plots showing mScI positive events after CRISPR transfections of pX459+guide negative control (left) or APC-mScI CRISPR constructs (right). The red gates in the right FACS plot indicate the 3 populations of mScI positive cells sorted (from left to right: low, middle & high). B) PCR results for mScI-APC sorted pools show the highest integration of mScI in the APC locus for the APC low populations. C) Graph depicting induction of *AXIN2* in the APC-mScI 'low' pool, as measured by qRT-PCR relative to *HPRT expression* and normalized to the BSA control. Bars represent the mean and the error bars represent the standard deviation of an n=3 technical replicate from n=1 experiment. Note that both WNT3A and CHIR induce *AXIN2* expression in this cell population. D) Representative confocal images comparing HEK293T wild-type cells with the APC-mScI 'low' pool. APC-mScI shows localization at the membrane and in the cytoplasm, compared to HEK293T WT which shows autofluorescence mostly in the cytoplasm and located in some punctae in the cells. Scalebar represents 10 µm.

DVL2

As DVL is the main link between the WNT receptor complex and inactivation of the destruction complex, we also generated CRISPR cell lines for DVL. We received HEK293 cells expressing endogenous DVL2-EGFP as a kind gift from the lab of Madelon Maurice. These cells showed a homogeneous cytoplasmic distribution with confocal microscopy, and not the typical punctae that are often observed (e.g. Schaefer et al. 2020). However, in the studies describing puncta there often is some (slight) overexpression of DVL, which could increase the presence of larger complexes. Indeed, when we overexpressed untagged DVL2 in these cell lines, DVL2-EGFP also localized to puncta, which was not the case upon overexpression of DVL2-ΔDIX (Figure 4A). This indicated that supraphysiological levels of DVL are required to form punctae in a DIX-dependent manner. This highlights the importance of maintaining endogenous levels, as even slight elevations can cause formation of structures that are not readily observed at the endogenous level. Of note, these observations do not exclude that different states of DVL2 might exist. For instance, it could appear either as mainly diffuse or mainly as punctae across different tissues and organisms due to different endogenous concentrations or presence of binding partners.

Next, we modified the constructs provided by the lab of Madelon Maurice in order to tag DVL2 with mScI in HAP1 cells. Following FACS sorting and locus-specific PCR we did detect successful integration of mScI at the endogenous DVL locus (Figure 4B-C). However, we also obtained some heterozygote clones, indicating that at least part of the HAP1 cell population was diploid at the time of sorting. It is known that HAP1 cells can become diploid over time, which can pose a problem for further downstream genome editing (Beigl et al. 2020).

FIGURE 4 (RIGHT): DVL2-mScI CRISPR cell line. A) Representative confocal images of HEK293 DVL-EGFP clone #10 (kindly provided by the lab of Madelon Maurice) transfected with a DVL2-WT or DVL2-ΔDIX overexpression plasmids. Overexpression of DVL2-WT induces punctae formation (see arrows), while overexpression of DVL2-ΔDIX does not. In absence of DVL2-WT overexpression DVL2 is diffusely localized in the cytoplasm and nucleus, although excluded from the nucleoli and some cytoplasmic organelles. Scale bar represents 10 µm. B) FACS plots showing mScI positive events after CRISPR transfections of pX459+guide negative control (left) or DVL2-mScI CRISPR constructs (right). C) DVL2 locus PCR for single cell clones obtained in (B). Several wildtype (WT) and homozygous (HOM) clones were identified, including clone #4.9 that is used in panels D and E. The presence of some heterozygous (HET) clones indicates that the population was not purely haploid at the time of sorting, so clones must be checked for haploid status if required for future work. In addition, clone #4.9 should be sequence verified if used for further studies. D) Representative confocal images from SGFP2-CTNNB1 clone #2 and DVL2-mScI clone #4.9 that were mixed prior to seeding in a 1:1 ratio. Two hours after treatment with WNT3A cytoplasmic and nuclear accumulation of SGFP2-CTNNB1 can be observed, but DVL2-localization does not appear altered. DVL2 appears mainly cytoplasmic in both stimulated and unstimulated conditions. Scale bar represents 10 µm. E) Graph depicting the induction of *AXIN2* as measured by qRT-PCR relative to HPRT expression and normalized to untreated SGFP2-CTNNB1 control. SGFP2-CTNNB1 clone #2 and DVL2-mScI clone #4.9 were treated for 24 hours with 100 ng/ml WNT3A. Vertical lines represent the standard deviation of a technical triplicate, individual data points represent independent biological replicates.

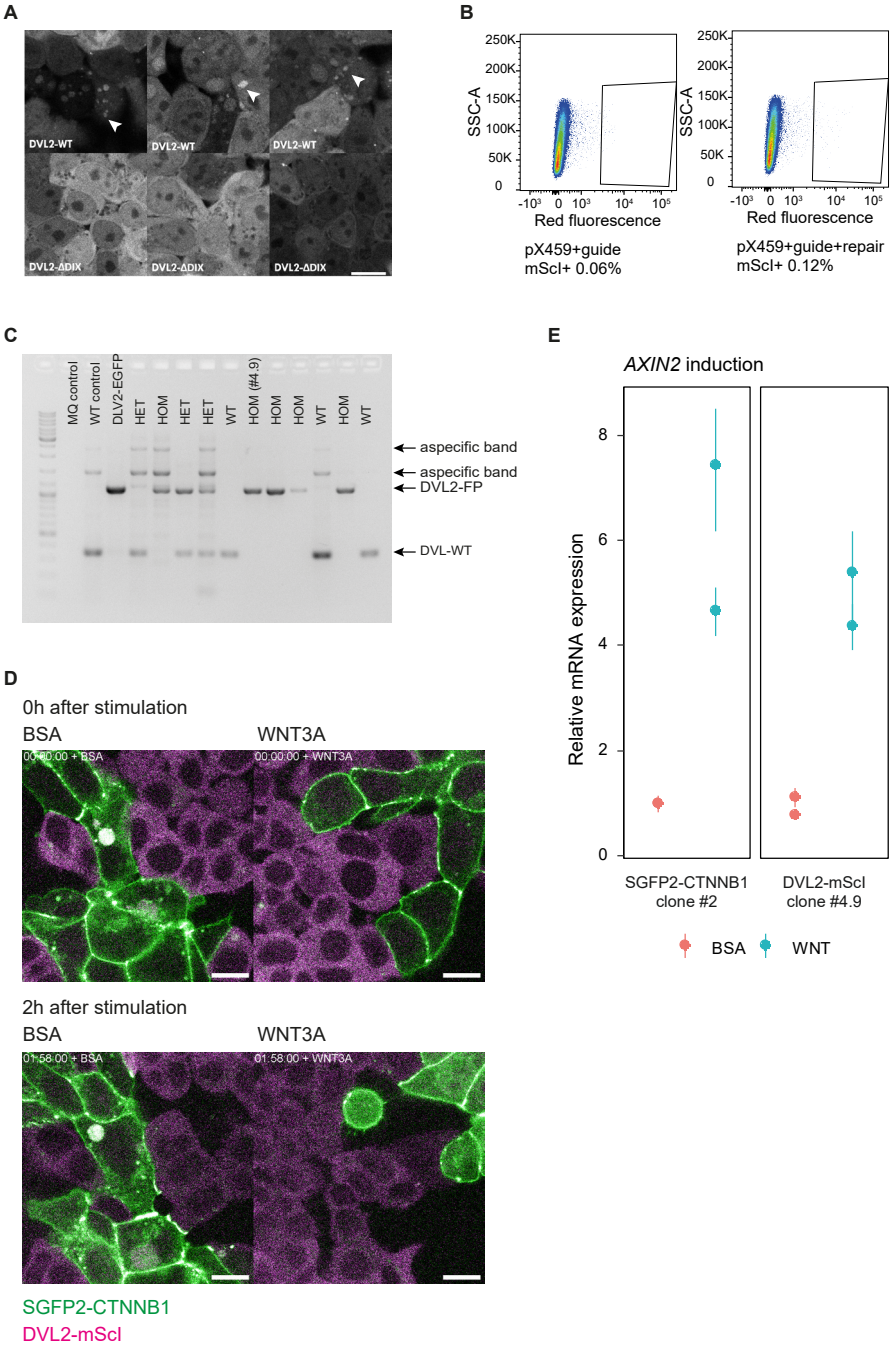
A
DVL2-WT
DVL2-WT
DVL2-WT
DVL2-ΔDIX
DVL2-ΔDIX
DVL2-ΔDIX
B
SSC-A
Red fluorescence
pX459+guide
mScI+ 0.06%
pX459+guide+repair
mScI+ 0.12%
C
MQ control
WT control
DLV2-EGFP
HET
HOM
HET
HET
WT
HOM (#4.9)
HOM
HOM
WT
HOM
WT
aspecific band
aspecific band
DVL2-FP
DVL-WT
D
0h after stimulation
BSA
WNT3A
00:00:00 + BSA
00:00:00 + WNT3A
2h after stimulation
BSA
WNT3A
01:58:00 + BSA
01:58:00 + WNT3A
SGFP2-CTNNB1
DVL2-mScI
E
AXIN2 induction
Relative mRNA expression
SGFP2-CTNNB1
clone #2
DVL2-mScI
clone #4.9
BSA
WNT

One of the homozygous DVL2-mScI clones (4.9) showed cytoplasmic distribution in unstimulated conditions (Figure 4D) similar to the localization of DVL-EGFP in HEK293 cells (Figure 4A). Upon stimulation with WNT3A, we did not observe any changes to the distribution of DVL2-mScI, even though SGFP2-CTNNB1 HAP1 cells in the same well reported that the WNT3A was active (Figure 4D, Movie 2). This suggests, that DVL2 does not undergo a major change in localization upon WNT ligand stimulation. The DVL2-mScI cells did show induction of *AXIN2* upon WNT3A treatment, demonstrating that the signaling function of DVL2 was intact in these cells (Figure 4E). At first glance, we were surprised to not see any membrane recruitment of DVL2, as DVL recruitment to the activated LRP5/6-FZD receptor complex has been described as an essential step (reviewed in Bienz 2014). However, studies with endogenously tagged DVL2 by other groups have shown that DVL2 recruitment is highly dynamic and due to high level of cytoplasmic DVL2 difficult to detect without specialized imaging techniques such as Total Internal Reflection Fluorescence microscopy (TIRF) where the membrane can be illuminated and imaged more selectively (Kan et al. 2020; Ma et al. 2020). We did not explore this avenue, but we envision that such techniques can be used to study DVL2 in our DVL2-mScI line further. First, this cell line could be used to confirm the limited recruitment and oligomer size of DVL2 at the plasma membrane upon ligand binding, as the two aforementioned studies have some discrepancies in their results on DVL recruitment. Additional tagging of for example CTNNB1 in this cell line, could also help to elucidate if complexes that contain both DVL2-mScI and CTNNB1 form upon WNT signaling, as would be expected from the previous identification of transducer complexes (Hagemann et al. 2014; Lybrand et al. 2019).

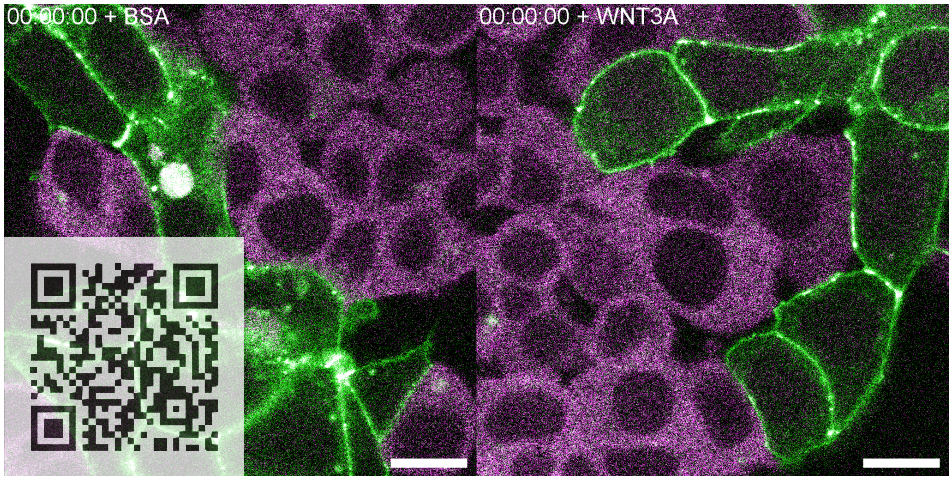

MOVIE 2: SGFP2-CTNNB1 and DVL2-mScI response to WNT3A. DVL2-mScI clone #4.9 (in magenta) and SGFP2-CTNNB1 clone #2 (in green) were mixed 1:1 at the time of seeding. At the start of imaging, cells were treated with 100 ng/ml WNT3A (right) or BSA control (left), time is indicated in the top left corners, the scale bar represents 10 µm. https://youtu.be/bmvgMscfgN0

GSK3

Finally, we focused on GSK3B as one of the main kinases in the destruction complex. We successfully tagged GSK3B with mScI in HAP1 cells (Figure 5A). These cells showed *AXIN2* induction upon treatment with WNT3A indicating that their pathway remained intact (Figure 5B). mScI-GSK3B showed a primarily cytoplasmic localization both before and after WNT3A treatment (Figure 5C, Movie 3). Again, neighboring SGFP2-CTNNB1 cells did show increases in intracellular intensity, showing the activity of the WNT3A added to these cultures. GSK3B has previously been described to enter into multivesicular bodies upon WNT3A treatment (Taelman et al. 2010), but we did not observe this – at least not in the form of any apparent accumulation of the fluorescent signal in structures resembling larger vesicles. The lack of visible sequestration of GSK3B into multivesicular bodies is consistent with a recent study (Rim et al. 2020) and suggests that this mechanism might not be universally required for WNT signaling.

Additionally, we generated a dual-color polyclonal cell line where CTNNB1 was tagged with SGFP2 and GSK3B was tagged with mScI. Of note, the parental SGFP2-CTNNB1 used for these experiments (a different line from the ones used in Chapter 3) was later identified out to have an additional mutation in intron 1 of CTNNB1. The dual color cell population showed the same cytoplasmic distribution of mScI-GSK3B and no clear changes in the signal intensity or localization upon WNT3A stimulation (Figure 5D, Movie 4). These cells did, however, show intracellular accumulation of CTNNB1 (Figure 5D) and a transcriptional response at the level of *AXIN2* (Figure 5B), indicating again that these cells had a functional WNT/CTNNB1 pathway.

We intended to use these dual color cells for fluorescence cross correlation spectroscopy (FCCS). As in FCS, as explained in Chapter 3, dynamics of fluorescently labeled particles (in this case mScI-GSK3B and SGFP2-CTNNB1) can be measured and their concentrations and diffusion kinetics can be determined. Additionally, by using the two different colors FCCS also allows a cross-correlation to be measured. If the fluorescent particles are moving together, due to direct or indirect binding, there will be a high cross-correlation between the two color signals. In contrast, if they are moving independently (i.e., they are not complexed), there will be no-cross correlation. We had hoped to use this technique to determine whether CTNNB1 and GSK3B were part of the same complex before and after WNT3A stimulation, as this would have provided additional proof that the cytoplasmic complex from Chapter 3 is indeed the destruction complex. However, we ran into technical difficulties and were unable to sufficiently separate the positive and negative controls (an SGFP2-GEFT-mScI and an SGFP2-T2A-mScI construct, which results in a fusion protein with predicted perfect cross-correlation and two dissociated proteins with predicted zero cross-correlation, respectively), and were not able to resolve those issue despite our best efforts (data not shown). However, this cell line would be suitable to further research the association and CTNNB1 and GSK3B at endogenous levels in an optimized FCCS setup.

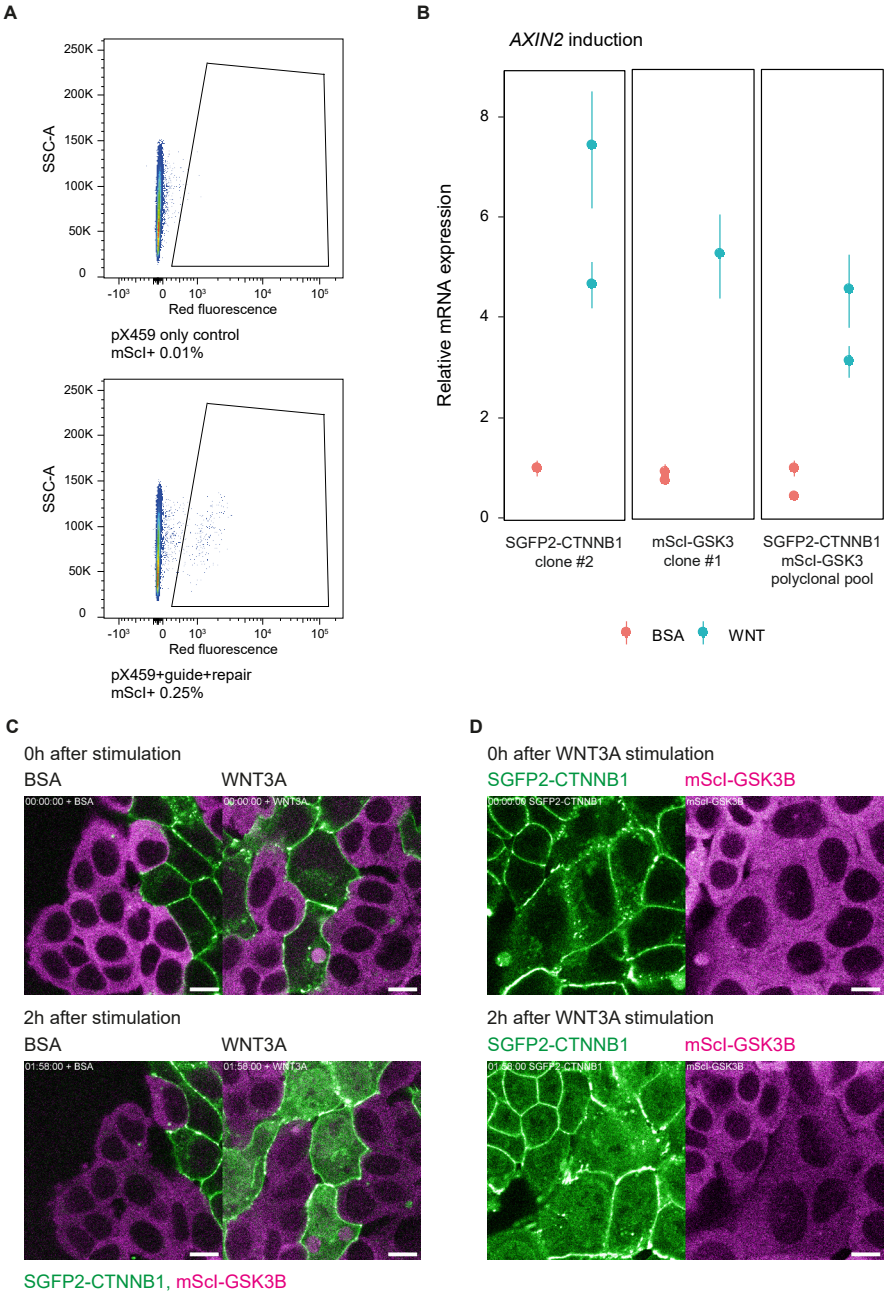

FIGURE 5: mScI-GSK3B CRISPR cell lines. A) FACS plots showing mScI positive events after CRISPR transfections of pX459 negative control (top) or mScI-GSK3B CRISPR constructs (bottom). Several clones positive for mScI-GSK3B were identified by PCR and sequenced verified by Sanger Sequencing. Clone #1 was selected for further experiments in B and C. B) Graph depicting the induction of *AXIN2* as by qRT-PCR relative to HPRT expression and normalized to untreated SGFP2-CTNNB1 control. SGFP2-CTNNB1 clone #2, mScI-GSK3B clone #1 and a polyclonal pool of SGFP2-

CTNNB1/mScI-GSK3B double positive cells (based on clonal cell line 3A9 for SGFP2-CTNNB1 which contains a small indel in the first intron of CTNNB1) were treated for 24 hours with 100 ng/ml WNT3A. Vertical lines represent the standard deviation of a technical triplicate, individual data points represent independent biological replicates. C) Representative confocal images from SGFP2-CTNNB1 clone #2 and mScI-GSK3B clone #1 that were mixed prior to seeding in a 1:1 ratio. Two hours after treatment with WNT3A cytoplasmic and nuclear accumulation of SGFP2-CTNNB1 can be observed, but mScI-GSK3B localization does not appear altered. mScI-GSK3B appears mainly cytoplasmic in both stimulated and unstimulated conditions. Scale bar represents 10 µm. D) Representative confocal images from a polyclonal pool of SGFP2-CTNNB1 /mScI-GSK3B double positive cells. Two hours after treatment with WNT3A cytoplasmic and nuclear accumulation of SGFP2-CTNNB1 can be observed, but mScI-GSK3B localization does not appear altered. mScI-GSK3B appears mainly cytoplasmic across the two hours of imaging. Scale bar represents 10 µm.

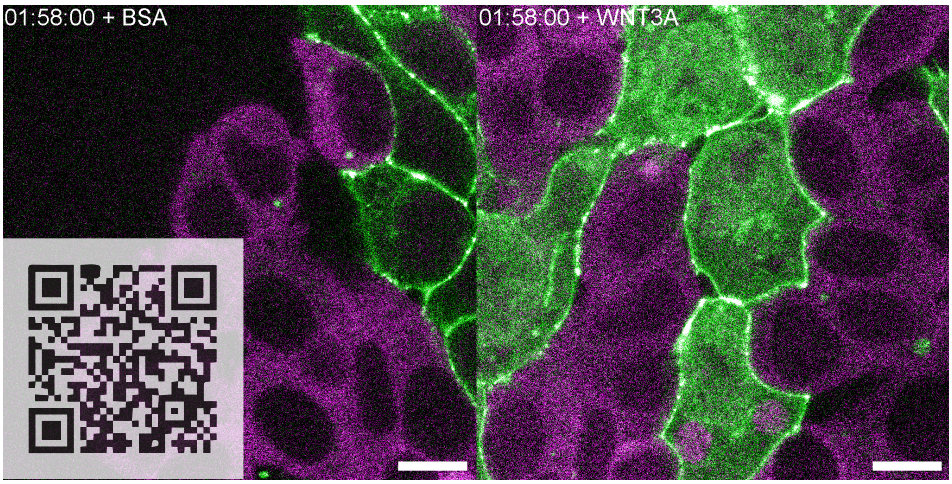

MOVIE 3: SGFP2-CTNNB1 and mScI-GSK3B response to WNT3A. mScI-GSK3B clone #1 (in magenta) and SGFP2-CTNNB1 clone #2 (in green) were mixed 1:1 at the time of seeding. At the start of imaging, cells were treated with 100 ng/ml WNT3A (right) or BSA control (left), time is indicated in the top left corners, the scale bar represents 10 µm. Use the QR-code to view the movie or visit https://youtu.be/DY-VH3tjZNE.

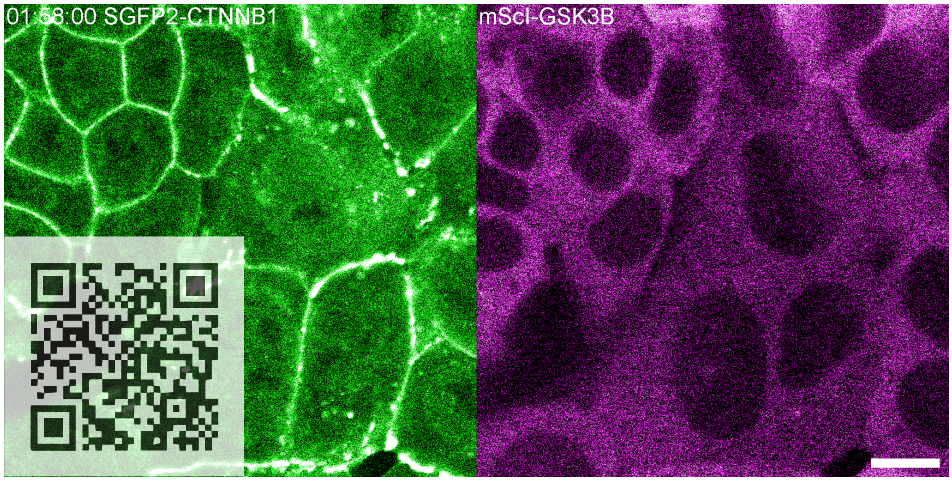

MOVIE 4: SGFP2-CTNNB1 /mScI-GSK3B response to WNT3A. This double positive polyclonal population of SGFP2-CTNNB1 (in green) and mScI-GSK3B (in magenta) was treated at the start of imaging with 100 ng/ml WNT3A, time is indicated in the top left corners, the scale bar represents 10 µm. Use the QR-code to view the movie or visit https://youtu.be/jU60npT2JmM.

A chemically-inducible dimerization system to study destruction complex interactions

As we could not confidently study interactions with FCCS with our local set up, we sought to develop different tools that we could use for this purpose. To this end, we exploited a chemically-inducible dimerization (CID) system. CID has been used as a cell biology tool for nearly 20 years. One widely used CID system utilizes FRB and FKBP12 domains, which very rapidly (on a timescale of seconds to minutes) and irreversibly heterodimerize into a rigid structure upon stimulation with membrane permeable rapamycin. Rapamycin-induced dimerization experiments have provided insight in several cellular processes by fusing FRB and FKBP12 with other proteins of interest (reviewed in Derose et al. 2013). For studying protein-protein interactions, one can induce the forced relocalization of one protein (the FKBP-12 fused bait) to a static cellular anchor site (fused to FRB) upon addition of rapamycin, while monitoring the co-relocalization of a presumed interacting protein (prey). This could also be described as an *in vivo* pull down. Relocalization of the 'prey-protein' to the anchor site indicates a direct or indirect protein-protein interaction between the prey and the bait (Figure 6A). When performed under live cell imaging conditions, binding affinities might be deduced from the kinetics of co-relocalization. Moreover, Fluorescence Recovery After Photobleaching (FRAP) measurements could be performed after co-relocalization to the anchor to further determine the kinetics of these interactions.

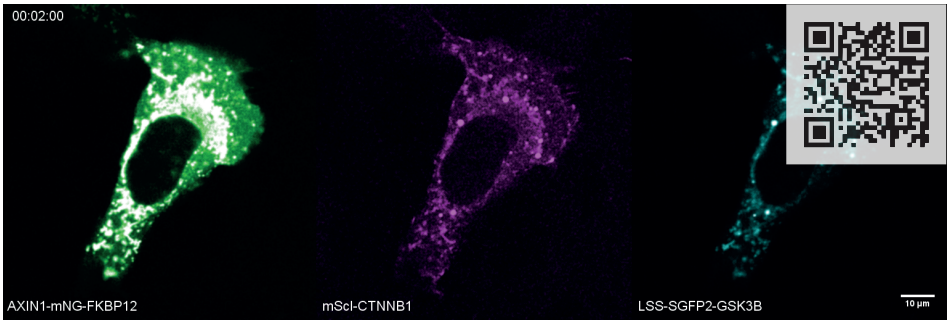

MOVIE 5: Co-relocalization of CTNNB1 and GSK3B with AXIN1. At 00:00:00 rapamycin is added which relocalizes AXIN1-mNG-FKBP12 to the mitochondrial FRB anchor. Due to their interactions with AXIN1, mScI-CTNNB1 and lssSGFP2-GSK3B are co-relocalized to the mitochondria as well. Use the QR-code to view the movie or visit https://youtu.be/N0-R8E0ATOI.

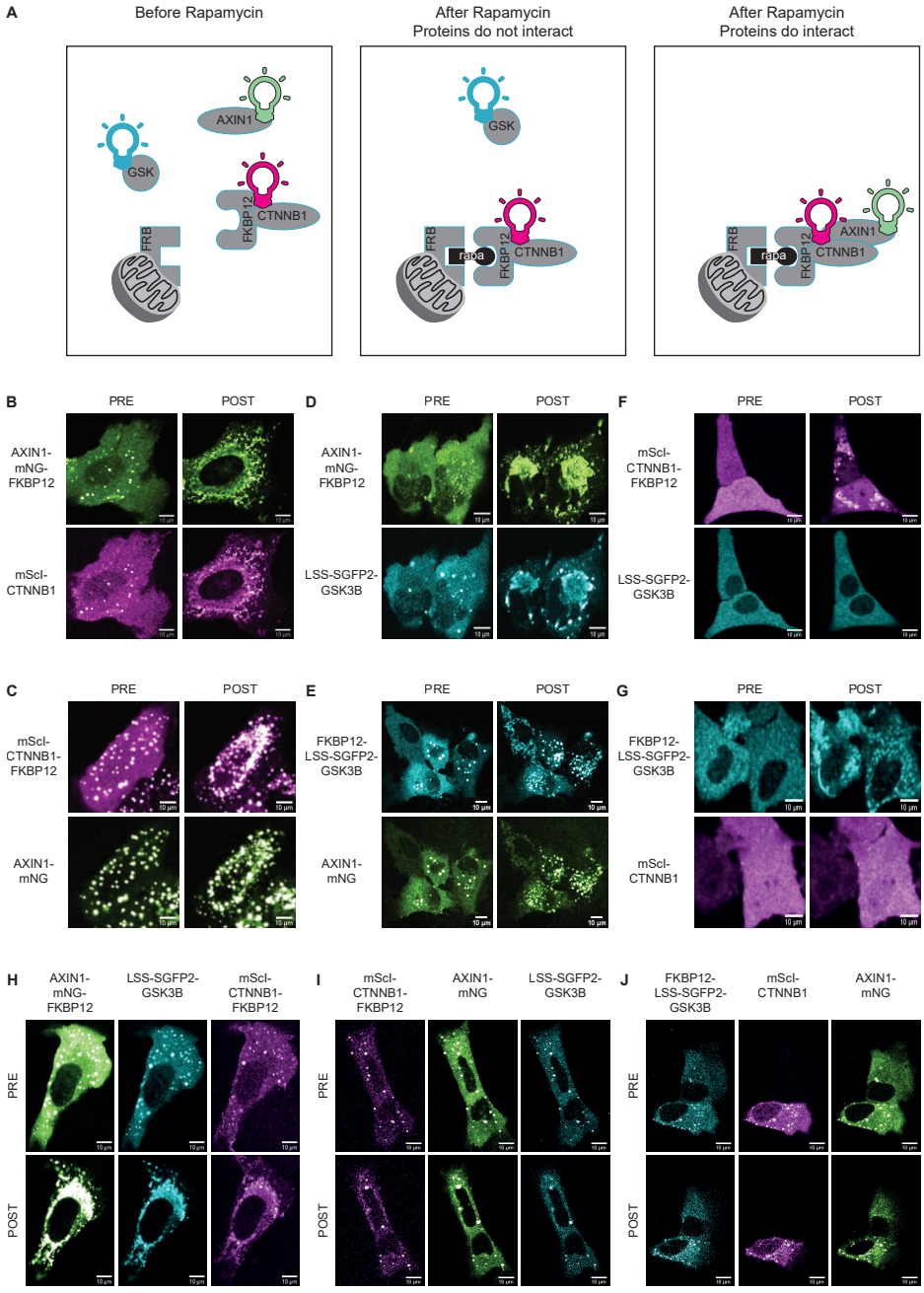

FIGURE 6: A rapamycin relocalization tool to study protein-protein interactions in the destruction complex. A) A schematic overview of protein relocalization with the rapamycin tool. The left panel shows the situation before addition of rapamycin. Tagged proteins are overexpressed in the cell and the anchor is located at the mitochondria. The next two panels show relocalization of FKBP12 proteins to the FRB anchor at the mitochondria induced by

rapamycin. When two proteins do not interact, for example CTNNB1 and GSK3, relocalization of one does not lead to co-relocalization of the other (middle panel). When two proteins do interact, for example CTNNB1 and AXIN1, relocalization of one does lead to co-relocalization of the other (right panel). In this way interactions of proteins can be studied in living cells. B-J) Representative confocal images of U2Os cells before and after rapamycin treatment with different combinations of GSK3, CTNNB1 and AXIN1 rapamycin constructs. Scale bar represents 10 µm. B) mScI-CTNNB1 co-relocalizes with AXIN1-mNG-FKBP12. C) AXIN1-mNG co-relocalizes with mScI-CTNNB1-FKBP12. D) lssSGFP2-GSK3B co-relocalizes with AXIN1-mNG-FKBP12. D) AXIN1-mNG co-relocalizes with FKBP12-lssSGFP2-GSK3B. E) lssSGFP2-GSK3B does not co-relocalize with mScI-CTNNB1. F) mScI-CTNNB1 does not co-relocalize with FKBP12-lssSGFP2-GSK3B. G) both mScI-CTNNB1 and lssSGFP2-GSK3B co-relocalize with AXIN1-mNG-FKBP12. H) both AXIN1-mNG and lssSGFP2-GSK3B co-relocalize with FKPB12-mScI-CTNNB1. I) Both AXIN1-mNG and mScI-CTNNB1 co-relocalize with FKBP12-lssSGFP2-GSK3B.

As a proof of principle, we established overexpression constructs for AXIN1, GSK3B and CTNNB1 containing a fluorescent fusion partner with or without the FKBP12 domain, and an anchor at the mitochondria (FRB-MoA). Relocalization of AXIN1-FKBP12 to the mitochondria, induced co-relocalization of both CTNNB1 and GSK3B, consistent with their known interaction (Figure 6B-E). In contrast, co-expression of CTNNB1 and GSK3B alone, with one of them coupled to the FKBP12 domain, did not induce co-relocalization (Figure 6F-G). This is consistent with the fact that GSK3B and CTNNB1 don't bind directly but only through AXIN1 (Chapter 2). In this overexpression experiment endogenous AXIN1 levels were presumably not sufficient to mediate this interaction. However, when AXIN1 was overexpressed in addition, this indirect interaction between CTNNB1 and GSK3B was restored (Figure 6 H-J, Movie 5).

This proof of principle shows that in an overexpression setting, we can probe the hierarchical interactions within the destruction complex. However, to address some of the open questions in the field, for example how interactions in the destruction complex change upon WNT stimulation, an endogenous version or low-level overexpression using lentiviral integration of this would be preferable, since elevated concentrations and disturbed ratios of the different signaling components, most likely can shift the interactions that are observed with this technique.

SUMMARY

In this addendum I have highlighted the work of Jasmijn Span, Sanne Lith, Beau Neep and Rianne Schoon who were students under my supervision. They put in a lot of effort to develop novel endogenously tagged cell lines for other components of the WNT/CTNNB1 pathway. Together we generated novel constructs for AXIN1, APC, GSK3B and DVL2, and were successful in tagging of the latter three. Interestingly, both GSK3B and DVL2 showed few changes in level and localization upon WNT3A addition, suggesting that for GSK3B multivesicular body formation might not be essential in all cell types and that DVL2 membrane localization is subtle and dynamic as measured by others as well. These experiments demonstrate that our CRISPR pipeline is applicable to other proteins, but at the same time highlights how finnicky it is to generate properly engineered cell lines as well, especially for lowly expressed proteins. Many studies have focused on increasing HDR (reviewed inBukhari and Müller 2019; Yang et al. 2020; Denes et al. 2021; Sun et al. 2022). Application of such strategies as well as addition of selection cassettes (Yan et al. 2020) or increased sensitivity to detect low fluorescence intensities, could help overcome the limitations we currently ran into.

Another goal was to combine this CRISPR labelling with our previously established SGFP2-CTNNB1 cell line and perform FCCS to identify the dynamic interactions between these proteins. Although we were able to generate dual tagged cells in this manner, we were unable to sufficiently separate positive and negative FCCS controls that were either covalently linked or separate proteins due to technical challenges. Therefore, we set up a novel system using a chemically inducible dimerization system to relocalize specific proteins to a defined location in the cell. Any interacting proteins are co-relocalized with this protein of interest, making this a *in vivo* pull-down system. In a proof of principle setup, we showed that CTNNB1 and GSK3B interact directly with AXIN1, and need AXIN1 to interact with each other. Further application of this system at overexpression and endogenous levels could offer new insights in the dynamic and hierarchical composition of the WNT/CTNNB1 destruction complex.

MATERIALS AND METHODS

All experimental procedures have been described in Chapter 3. Any deviations and additions are described below.

Constructs

Constructs were generated using conventional digestion and ligation-based cloning or Gibson cloning as described in Chapter 3. All inserts into vectors were sequence verified before use. Full sequences for newly generated constructs are available at https://osf.io/tfrsz/. Table 1 describes newly cloned constructs; Table 2 describes existing plasmids used in this addendum and Table 3 describes primers and oligos used.

TABLE 1: Newly cloned constructs

Construct	LMC #	RVA #	Backbone	Insert	primers to PCR insert	RE used	Remarks
FKBP12-LssSGFP2-C1	4943	pRVA277	FKBP12-mTq2-C1 (LMC3370)	LssSGFP2-C1 (LMC2293)	NA	AgeI/ BsrGI	
N1-LssSGFP2-FKBP12	4944	pRVA278	mTq2-FKBP12-N1 (LMC3373)	LssSGFP2-C1 (LMC2293)	NA	AgeI/ BsrGI	
FKBP12-mScI-C1	5237	pRVA290	FKBP12-mTq2-C1 (LMC3370)	mScI-C1 (LMC4604)	NA	AgeI/ BsrGI	
N1-mScI-FKBP12	5238	pRVA291	mTq2-FKBP12-N1 (LMC3373)	mScI-C1 (LMC4604)	NA	AgeI/ BsrGI	
FKBP12-mNG-C1	4947	pRVA281	FKBP12-mTq2-C1 (LMC3370)	mNG-C1 (LMC2326)	NA	AgeI/ BsrGI	
N1-mNG-FKBP12	4948	pRVA282	mTq2-FKBP12-N1 (LMC3373)	mNG-C1 (LMC2326)	NA	AgeI/ BsrGI	
FKBP12-mKOkappa-C1	4945	pRVA279	FKBP12-mTq2-C1 (LMC3370)	mKOk-C1 (LMC2239)	NA	AgeI/ BsrGI	not shown in this addendum, extra colour option for rapamycin experiments.
N1-mKOkappa-FKBP12	4946	pRVA280	mTq2-FKBP12-N1 (LMC3373)	mKOk-C1 (LMC2239)	NA	AgeI/ BsrGI	not shown in this addendum, can be used as extra colour for rapamycin experiments.
AXIN1-mNG	4956	pRVA205	mNG-C1 (LMC2326)	AXIN1-mNG-FKBP12-N1 (4949)	NA	EcoRI/ AgeI	
AXIN1-mNG-FKBP12	4949	pRVA200	mNG-FKBP12-N1 (LMC 4948)	Flag-Axin1 (LMC4934, addgene 109370)	RVA2718 & RVA2719	EcoRI/ AgeI	
AXIN1-deltaDix-mNG-FKBP12	4955	pRVA204	mNG-FKBP12-N1 (LMC4944)	Flag-Axin1 (LMC4934, addgene 109370)	RVA2718 & RVA 3353	EcoRI/ AgeI	not shown in this addendum, can be used to reduce oligo-merization of DVL2 in rapa-mycin studies

Construct	LMC #	RVA #	Backbone	Insert	primers to PCR insert	RE used	Remarks
mScI-CTNNB1	4950	pRVA201	mScI-C1 (LMC4604)	pT3-EF1aH N90 b-catenin (RvA80, addgene86499)	RVA2720 & RVA2721	BsrGI/ BamHI	
FKBP12-mScI-CTNNB1	4954	pRVA203	mScI-CTNNB1-C1 (LMC5238)	FKBP12-mScI-C1 (LMC5237)	NA	BsrGI/ BamHI	
lssSGFP2-GSK3B	4951	pRVA202	LssSGFP2-C1 (LMC2132)	HA GSK3 beta wt pcDNA3 (LMC4931, addgene14753)	RVA2722 & RVA 2723	BsrGI/ BglII	
FKBP12-lssSGFP2-GSK3B	4957	pRVA206	FKBP12-LSS-SGFP2-C1 (LMC4943)	LSS-SGFP2-GSK3B-C1 (LMC4951)	NA	BsrGI/ BglII	
APC-mTq2	4953	pRVA172	pmTq2-N1 (LMC 3863, RVA045)	pCMV-Neo-Bam APC (LMC4933)	backbone: RVA3138 & RVA3139, insert: RVA3140 & RVA3141	NA (Gibson cloning)	not shown in this addendum, can be used in rapamycin experiments
AXIN1-mScI repair	NA	pRVA133	AXIN1-mCherry (RvA119, Kind gift of Nicola Fenderico/ Madelon Maurice)	C1-mScarlet-i (LMC4604, RvA074)	Backbone: RVA 1608 & 1609, FP: 1610 &1611	NA (Gibson cloning)	Contains several variants compared to RefSeq that are known in HEK293 from which it was cloned
pX459-APC	NA	pRVA225	pX459 (pRVA047)	annealed oligos RVA2360 & 2361	NA	BbsI	
pRepair-APC-mSCI	4952	pRVA171	pBluescript II KS(+) (pRVA039)	HEK genomic DNA, RvA074 (LMC4604)	Backbone: RVA586 & RVA587, mScI: RVA3048 & RVA3049, left HR: RVA3046 & RVA3047, right HR: RVA3050 & RVA3051	NA (Gibson cloning)	not mutated PAM/gRNA so can lead to indels in repaired allele
DVL2-mSci repair	NA	pRVA147	DVL2-eGFP (RvA121, Kind gift of Nicola Fenderico/ Madelon Maurice)	C1-mScarlet-i (LMC4604, RvA074)	Backbone: RVA1612 & RVA 1613, FP: RVA1614 & RVA1615	NA (Gibson cloning)	
pX459-GSK3B	NA	pRVA127	pX459 (pRVA047)	annealed primers RVA1530 & RVA1531	NA	BbsI	
mSci-GSK3B repair	NA	pRVA136	pBluescript II KS(+) (RvA39)	HR: HAP1 gDNA, mScI: C1-mScarlet-i (LMC4604, RvA074)	Gibson [backbone: RVA 586 & RVA587, left HR: RVA1602 & RVA1603, mScI: RVA1604 & RVA1605, right HR: RVA1606 & RVA 1607], gRNA/PAM mutagenesis [RVA1751 & RVA1752]	NA (Gibson cloning)	

TABLE 2: Existing constructs

Construct	RVA #	LMC #	Addgene #	Remarks
mKOk-C1	NA	LMC2239	NA	Kind gift from Dorus Gadella
pX459 v2.0	pRVA047	NA	62988	Kind gift from Feng Zhan (Ran et al. 2013)
C1-mScarlet-i	pRVA074	LMC4604	85044	Kind gift from Dorus Gadella (Bindels et al. 2017)
pT3-EF1aH N90 b-catenin	pRvA080	NA	109370	Kind Gift from gift from Xin Chen (Tward et al. 2007)
pCS2-DVL2-WT	pRVA091	NA	NA	Kind gift from Xi He
pCS2-DVL2-deltaDix	pRVA092	NA	NA	Kind gift from Xi He
px459 DVL2 guide (GGTGTTTGAGGAGGTTCGAG)	pRVA119	NA	NA	Kind gift from Madelon Maurice
pX459 AXIN1 guide (CTAATCTCCGAGCCCACCCA)	pRVA120	NA	NA	Kind gift from Madelon Maurice
repair hs DVL2-eGFP	pRVA121	NA	NA	Kind gift from Madelon Maurice
repair hs AXIN1-mCherry	pRVA122	NA	NA	Kind gift from Madelon Maurice
pRepair-mScI-CTNNB1	pRVA130	NA	153431	see Chapter 3 for cloning details
mSci-T2A-sGFP2	pRVA145	LMC2669	NA	Kind gift from Dorus Gadella, FCCS controls, no data shown in this addendum
mSci-GEFT-sGFP2	pRVA146	LMC2670	NA	Kind gift from Dorus Gadella, FCCS controls, no data shown in this addendum
pX459-CTNNB1-ATG	pRVA148	NA	153429	see Chapter 3 for cloning details
FRB-CFP(w66a)-FRB-MoA	pRVA207	LMC4006	NA	Kind gift from Dorus Gadella
HA GSK3 beta wt pcDNA3	pRVA265	LMC4931	14753	Kind gift from Jim Woodgett (He et al. 1995)
Flag-Axin1	pRVA268	LMC4934	86499	Kind gift from Mariann Bienz (Fiedler et al. 2011)
FKBP12-mTq2-C1	pRVA288	LMC3370	NA	Kind gift from Dorus Gadella
mTq2-FKBP12-N1	pRVA289	LMC3373	NA	Kind gift from Dorus Gadella
mNG-N1	pRVA293	LMC2326	NA	Kind gift from Dorus Gadella

TABLE 3: Oligos and primers used in cloning of Table 1.

RVA primer #	Sequence
RVA2718	actggaattcgccaccatgaatatccaagagca
RVA2719	actgaccggtccaccgccacctccgtccaccttctccacttt
RVA 3353	actgaccggtccaccgccacctccgtacgccacaacgatgct
RVA2720	actgtgtacaagatggctactcaagctgattt
RVA2721	actgggatcctacaggtcagtatcaaaccagg
RVA2722	actgtgtacaagatgtcagggcggcccaga
RVA2723	actgagatctctaagtggagttggaagctgatgcag
RVA3138	ACCGGTCGCCACCATGGTGAG
RVA3139	CCGGGCCCGCGGTACCGT
RVA3140	CGACGGTACCGCGGGCCCGGGGATCCATGGCTGCAGCTTCATATG
RVA3141	GTAGAAGTTTGTATACAGGCAGCTGACTTGGTTTCCTTG
RVA1530	CATGCTGCCAAAAGCTGA
RVA1531	aaacTCAGCTTTTGGCAGCATGAAC
RVA1608	ctcgcccttgctcacTCCACCGCCACCTCCGTC
RVA1609	(gacgagctgtacaagGGAGGTGGCTACCCATACGATG
RVA1610	(tgggtagccacctccCTTGTACAGCTCGTCCAT
RVA1611	ggaggtggcggtggaGTGAGCAAGGGCGAG
RVA586	(AAGGCAAAATACGGACAAATTAGAT
RVA587	TCTCAAAACTGCATTCTGACTTTCA
RVA3048	CATCTGTTGGAGGTGGCGGTGGAATGGTGAGCAAGGGCGAG
RVA3049	CTCTTTTACTTGTACAGCTCGTCCATGC
RVA3046	GGGCGAATTGGAGCTACGTGAGCACAGCAAACATTC
RVA3047	TCCACCGCCACCTCCAACAGATGTCACAAGGTAAGACC
RVA3050	AGCTGTACAAGTAAAAGAGAGGAAGAATGAAAC
RVA3051	GCGGTGGAGCTAGCTGAAACAAGACCCTTCAAAC
RVA1612	gacgagctgtacaagGGAGGTGGCGATTACAAGGATG
RVA1613	ctcgcccttgctcacTCCACCGCCACCTCCCAT
RVA1614	GGAGGTGGCGGTGGAGTGAGCAAGGGCGAGG
RVA1615	GTAATCGCCACCTCCCTTGTACAGCTCGTCCATGC
RVA1602	ctatagggcgaattggagctGGCCAAGTGACAAAGGAAG
RVA1603	tgctcaccatGATCACTCTCTTCGCGAATC
RVA1604	gagagtgatcATGGTGAGCAAGGGCGAG
RVA1605	gccctgacatCTTGTACAGCTCGTCCATGC
RVA1606	gctgtacaagATGTCAGGGCGGCCCAGA
RVA1607	agcggccgccaccgcggtggTAAGGAACCCGCCAGAACATTTAACAG
RVA1751	CCGGTGCAGCAGCCTAGTGCTTTTGGCAGCATG
RVA1752	CATGCTGCCAAAAGCACTAGGCTGCTGCACCGG
RVA2360	CACCGTGACATCTGTTTAAAAGAG
RVA2361	AAACCTCTTTTAAACAGATGTCAC

Overview CRISPR cell lines

New HAP1 cell lines were generated as previously described in Chapter 3. All lines used and generated are listed below in Table 4.

TABLE 4: Cell lines

Parental cell line	Genotype	Clone #	Generation	Remarks
HEK293T	AXIN1-mCherry	#5	Kind gift of Madelon Maurice	AXIN1-mCherry was not visible by confocal microscopy.
HEK293T	AXIN1-mCherry DVL2-EGFP	#10	Kind gift of Madelon Maurice	AXIN1-mCherry was not visible by confocal microscopy.
HAP1	mScI-CTNNB1	#9	As in Chapter 3, using pRepair-mScI-CTNNB1 (pRVA130) and pX459-CTNNB1-ATG (pRVA148)	Cell line was verified by PCR, Sanger Sequencing, *AXIN2* qRT-PCR and confocal microscopy.
HAP1	DVL2-mScI	#4.16	As in Chapter 3, using DVL2-mSci repair (pRVA147) and px459 DVL2 guide (pRVA119)	Cell line was verified by PCR, AXIN2 qRT-PCR and confocal microscopy. Sanger Sequencing is not yet performed and ploidy status is not confirmed but might be diploid since other clones were heterozygous.
HAP1	mScI-GSK3B	#1	As in Chapter 3, pX459-GSK3B (pRVA127) and mSci-GSK3B repair (hs) (pRVA136)	Cell line was verified by PCR, Sanger Sequencing, AXIN2 qRT-PCR and confocal microscopy.
HAP1 SGFP2-CTNNB1 clone 3A9	SGFP2-CTNNB1 ; mScI-GSK3B	Polyclonal sorted population	As in Chapter 3, pX459-GSK3B (pRVA127) and mSci-GSK3B repair (hs) (pRVA136)	Cell population contains an indel in the first intron of SGFP2-CTNNB1 like its parental clone A9. Cell line was verified by PCR, AXIN2 qRT-PCR and confocal microscopy. Sanger Sequencing of the polyclonal mScI-CTNNB1 locus was not performed.

For AXIN-mScI HAP1 trials, AXIN1-mScI repair (pRVA133) and pX459 AXIN1 guide (pRVA120) were used according to the pipeline in Chapter 3, but no positive cells could be isolated with FACS.

For APC-mScI HEK cell populations, a similar CRISPR/Cas9 pipeline (Chapter 3) was followed with minor adaptations. Here, 150,000 cells were seeded in 6-well plates and transfected with a total of 1500 ng DNA per well and 4.5 µg Polyethyleneimine (PEI). Selection for transfection was performed with 1.5 µg/ml Puromycin. Polyclonal APC-mScI populations were not kept as it was revealed that most derived clones contained indels at the C-terminus.

Live cell imaging of CRISPR clones

Live cell imaging on CRISPR clones was performed in 8-well glass Ibidi slides on a Leica SP8 as described in Chapter 3 with the following modifications. When two cell lines were mixed 44.000 cells of both cell lines were mixed and added per well. The time interval was 2 minutes and the resolution was 1024*1024 pixels (pixel size: 61.51 µm). Channels were

captured sequentially. SGFP2 was excited with a 488 laser and detected with a HyD detector at 495 nm – 555 nm; mScI was excited with a 561 laser, and detected with a HyD detector at 568 nm – 628 nm, SiR-DNA (not shown) was excited with a 633 laser, and detected with a HyD detector at 640 nm - 740 nm. Images are represented using the FSP LUTs developed by Marten Postma. These LUTs range from black, to a chosen color, to white to better represent the range of intensities compared to two-color LUTs (Figure 7).

FIGURE 7: FSP magenta (left) and FSP green (right) LUTs ranging from lowest intensity (left, black) to highest intensity (right, white).

Rapamycin experiments.

All rapamycin experiments were performed with U2OS cells. U2OS osteosarcoma cells were cultured at 37°C and 5% CO2 in Dulbecco's Modified Eagle Medium (DMEM; Gibco 11965092) supplemented with 10% FBS. Cells were split every 3-4 days at ~90% confluency. For live cell microscopy, cells were seeded 1, 2, or 3 days prior at glass cover slips in 6-wells plates at 100,000, 50,000, or 20,000 cells per well, respectively. Cells were transfected the day before imaging with 500 or 1000 ng DNA, 4.5 or 9 µg PEI (polyethyleneimine) in MQ, respectively, mixed in 50 µL reduced serum medium (Opti-MEM; Gibco 51985034) and added in a dropwise fashion.

Confocal microscopy experiments were performed on a Leica SP8 machine with LAS X software (Leica Microsystems B.V.). Rapamycin images and movies were acquired at RT with an HC Plan Apo 63x NA1.4 oil objective using sequential scanning. LssSGFP2 was excited with a 405 laser, and detected with a PMT at 500 nm - 540 nm, mNG was excited with a 488 laser and detected in the same PMT as LssSGFP2 (505 nm – 548 nm), mScI was excited with a 561 laser, and detected with a PMT at 581 nm-651 nm. Images were acquired at 1024*1024 resolution and averaging of 4 frames before and after the movie sequence. Movies were acquired at 512*512 resolution without averaging. Rapamycin dynamics movies consisted of 5 pre-administration frames as a baseline after which rapamycin was administered to the imaging ring within 2 frames of measurement to 100 nM final concentration, followed by 115 frames (9.5) minutes of measurement at 5-second intervals.

AUTHOR CONTRIBUTIONS

Saskia M.A. de Man, conceptualization, direct supervision of student projects, experimentation (support of students in cell culture, cloning, FACS sorting, microscopy and qPCR), original manuscript preparation.

Jasmijn M. Span (BSc student at the time), experimentation (cloning of CRISPR constructs).

Sanne C. Lith (MSc student at the time), experimentation (cloning of CRISPR constructs, generation of mScI-CTNNB1, mScI-GSK3B and DVL2-mScI cell lines, FCCS).

Beau Neep (BSc student at the time), experimentation (cloning of CRISPR constructs, generation, genotyping, qPCR and imaging of APC-mScI HEK293 polyclonal lines).

Rianne M. Schoon (MSc student at the time), experimentation (cloning of rapamycin constructs, all rapamycin experiments).

Marten Postma, conceptualization of rapamycin studies, co-supervision of Rianne Schoon.

Mark A. Hink, conceptualization of FCCS studies, co-supervision of Sanne Lith, manuscript review and editing.

Renée van Amerongen, co-supervision of all students, manuscript review and editing.

ACKNOWLEDGEMENTS

We thank Nicola Fenderico and Madelon Maurice for the DVL2-EGFP and AXIN1-mCherry constructs and cell lines. We thank the van Leeuwenhoek Centre for Advanced Microscopy (LCAM, Section Molecular Cytology, Swammerdam Institute for Life Sciences, University of Amsterdam) for the use of their facilities and LCAM staff for sharing their expertise and providing technical support. We thank Lars van Oerthel and Gonzalo Congrains Sotomayor for the support of all FACS experiments. We thank Anna Chertkova for organizing and teaching the cloning class. We thank all current and former lab members and students of DSCCB led by dr. Renée van Amerongen and Molecular Cytology led by prof. dr. Dorus Gadella.

BIBLIOGRAPHY

Beigl TB, Kjosås I, Seljeseth E, et al (2020) Efficient and crucial quality control of HAP1 cell ploidy status. Biol Open 9:bio057174. https://doi.org/10.1242/bio.057174

Bienz M (2014) Signalosome assembly by domains undergoing dynamic head-to-tail polymerization. Trends Biochem Sci 39:487–495. https://doi.org/10.1016/j.tibs.2014.08.006

Bindels DS, Haarbosch L, van Weeren L, et al (2017) mScarlet: a bright monomeric red fluorescent protein for cellular imaging. Nat Methods 14:53–56. https://doi.org/10.1038/nmeth.4074

Bukhari H, Müller T (2019) Endogenous fluorescence tagging by CRISPR. Trends Cell Biol 29:912–928. https://doi.org/10.1016/j.tcb.2019.08.004

Denes CE, Cole AJ, Aksoy YA, et al (2021) Approaches to enhance precise CRISPR/Cas9-mediated genome editing. Int J Mol Sci 22:8571. https://doi.org/10.3390/ijms22168571

Derose R, Miyamoto T, Inoue T (2013) Manipulating signaling at will: Chemically-inducible dimerization (CID) techniques resolve problems in cell biology. Pflugers Arch Eur J Physiol 465:409–417. https://doi.org/10.1007/s00424-012-1208-6

Fiedler M, Mendoza-Topaz C, Rutherford TJ, et al (2011) Dishevelled interacts with the DIX domain polymerization interface of Axin to interfere with its function in down-regulating β-catenin. Proc Natl Acad Sci U S A 108:1937–1942. https://doi.org/10.1073/pnas.1017063108

Hagemann AIH, Kurz J, Kauffeld S, et al (2014) In-vivo analysis of formation and endocytosis of the Wnt/β-Catenin signaling complex in zebrafish embryos. J Cell Sci 3970–3982. https://doi.org/10.1242/jcs.148767

Hankey W, Frankel WL, Groden J (2018) Functions of the APC tumor suppressor protein dependent and independent of canonical WNT signaling: implications for therapeutic targeting. Cancer Metastasis Rev 37:159–172. https://doi.org/10.1007/s10555-017-9725-6

He X, Saint-Jeannet JP, Woodgett JR, et al (1995) Erratum: Glycogen synthase kinase-3 and dorsoventral patterning in Xenopus embryos (Nature (1995) 374 (617-622)). Nature 375:253. https://doi.org/10.1038/375253a0

Jiang S, Zhang M, Sun J, Yang X (2018) Casein kinase 1α: Biological mechanisms and theranostic potential. Cell Commun Signal 16:1–24. https://doi.org/10.1186/s12964-018-0236-z

Kan W, Enos MD, Korkmazhan E, et al (2020) Limited dishevelled/axin oligomerization determines efficiency of wnt/b-catenin signal transduction. Elife 9:1–33. https://doi.org/10.7554/eLife.55015

Kitazawa M, Hatta T, Ogawa K, et al (2017) Determination of rate-limiting factor for formation of beta-catenin destruction complexes using absolute protein quantification. J Proteome Res 16:3576–3584. https://doi.org/10.1021/acs.jproteome.7b00305

Lee E, Salic A, Krüger R, et al (2003) The roles of APC and axin derived from experimental and theoretical analysis of the Wnt pathway. PLoS Biol 1:116–132. https://doi.org/10.1371/journal.pbio.0000010

Lybrand DB, Naiman M, Laumann JM, et al (2019) Destruction complex dynamics: Wnt/β-catenin signaling alters Axin-GSK3β interactions in in vivo. Development 146:dev164145. https://doi.org/10.1242/dev.164145

Ma W, Chen M, Kang H, et al (2020) Single-molecule dynamics of dishevelled at the plasma membrane and Wnt pathway activation. Proc Natl Acad Sci U S A 117:16690–16701. https://doi.org/10.1073/pnas.1910547117

Parker TW, Neufeld KL (2020) APC controls Wnt-induced β-catenin destruction complex recruitment in human colonocytes. Sci Rep 10:1–14. https://doi.org/10.1038/s41598-020-59899-z

Ran FA, Hsu PD, Wright J, et al (2013) Genome engineering using the CRISPR-Cas9 system. Nat Protoc 8:2281–308. https://doi.org/10.1038/nprot.2013.143

Rim EY, Kinney LK, Nusse R (2020) β-catenin-Mediated Wnt Signal Transduction Proceeds Through an Endocytosis-Independent Mechanism. bioRxiv 1–16. https://doi.org/10.1101/2020.02.13.948380

Robertson H, Hayes JD, Sutherland C (2018) A partnership with the proteasome; the destructive nature of GSK3. Biochem Pharmacol 147:77–92. https://doi.org/10.1016/j.bcp.2017.10.016

Schaefer KN, Pronobis MI, Williams CE, et al (2020) Wnt regulation: exploring Axin-Disheveled interactions and defining mechanisms by which the SCF E3 ubiquitin ligase is recruited to the destruction complex. Mol Biol Cell 31:992–1014. https://doi.org/10.1091/mbc.E19-11-0647

Sun W, Liu H, Yin W, et al (2022) Strategies for enhancing the homology-directed repair efficiency of CRISPR-Cas systems. Cris J 5:7–18. https://doi.org/10.1089/crispr.2021.0039

Taelman VF, Dobrowolski R, Plouhinec JL, et al (2010) Wnt signaling requires sequestration of Glycogen Synthase Kinase 3 inside multivesicular endosomes. Cell 143:1136–1148. https://doi.org/10.1016/j.cell.2010.11.034

Tward AD, Jones KD, Yant S, et al (2007) Distinct pathways of genomic progression to benign and malignant tumors of the liver. Proc Natl Acad Sci U S A 104:14771–14776. https://doi.org/10.1073/pnas.0706578104

Valenta T, Hausmann G, Basler K (2012) The many faces and functions of β-catenin. EMBO J 31:2714–2736. https://doi.org/10.1038/emboj.2012.150

van Kappel EC, Maurice MM (2017) Molecular regulation and pharmacological targeting of the β-catenin destruction complex. Br J Pharmacol 174:4575–4588. https://doi.org/10.1111/bph.13922

Yan N, Sun Y, Fang Y, et al (2020) A universal surrogate reporter for efficient enrichment of CRISPR/Cas9-mediated homology-directed repair in mammalian cells. Mol Ther - Nucleic Acids 19:775–789. https://doi.org/10.1016/j.omtn.2019.12.021

Yang H, Ren S, Yu S, et al (2020) Methods favoring homology-directed repair choice in response to crispr/cas9 induced-double strand breaks. Int J Mol Sci 21:1–20. https://doi.org/10.3390/ijms21186461